Electronic properties of adsorbates on $\mathrm{Ga\,As\,(001)}\text{-}c\,(2\times 8)\,/\,(2\times 4)$ ⊘

Darby L. Winn; Michael J. Hale; Tyler J. Grassman; Jonathan Z. Sexton; Andrew C. Kummel; Matthias Passlack; Ravi Droopad

Check for updates

View Online   Export Citation
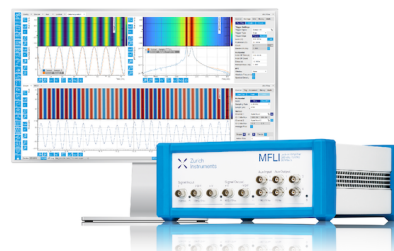
Electronic properties of adsorbates on GaAs(001)-*c*(2×8)/(2×4)

Darby L. Winn, Michael J. Hale, Tyler J. Grassman, Jonathan Z. Sexton, and
Andrew C. Kummel[a)]
*Department of Chemistry and Biochemistry, University of California, San Diego, La Jolla,
California 92093, USA*

Matthias Passlack and Ravi Droopad
Freescale Semiconductor, Inc., Tempe, Arizona 85284, USA

A systematic experimental and theoretical study was performed to determine the causes of oxide-induced Fermi level pinning and unpinning on GaAs(001)-$c(2\times8)/(2\times4)$. Scanning tunneling spectroscopy (STS) and density functional theory (DFT) were used to study four different adsorbates' (O_2, In_2O, Ga_2O, and SiO) bonding to the GaAs(001)-$c(2\times8)/(2\times4)$ surface. The STS results revealed that out of the four adsorbates studied, only one left the Fermi level unpinned, Ga_2O. DFT calculations were used to elucidate the causes of the Fermi level pinning. Two distinct pinning mechanisms were identified: direct (adsorbate induced states in the band gap region) and indirect pinnings (generation of undimerized As atoms). For O_2 dissociative chemisorption onto GaAs(001)-$c(2\times8)/(2\times4)$, the Fermi level pinning was only indirect, while direct Fermi level pinning was observed when In_2O was deposited on GaAs(001)-$c(2\times8)/(2\times4)$. In the case of SiO on GaAs(001)-$c(2\times8)/(2\times4)$, the Fermi level pinning was a combination of the two mechanisms. © *2007 American Institute of Physics*. [DOI: 10.1063/1.2786097]

I. INTRODUCTION

Over the last three decades, multiple successful/unsuccessful attempts have been made to construct a GaAs-based metal-oxide-semiconductor field effect transistor (MOSFET) device.[1–8] A GaAs-based MOSFET could potentially provide lower leakage current and lower standby power than current GaAs metal-semiconductor field effect transistors and high electron mobility transistors. In order to develop a GaAs-based MOSFET device with the best possible device characteristics, it is important to understand and characterize the oxide/GaAs interface at the molecular level. Having a molecular understanding of the interface facilitates the selection of the best oxide for a GaAs-based MOSFET device.

Scanning tunneling microscopy (STM) and density functional theory (DFT) are two surface science techniques that can be used to achieve a molecular understanding of adsorbate/semiconductor surfaces. STM can be used to image both the clean semiconductor surfaces and adsorbate covered semiconductor surfaces; thereby facilitating initial assignments of adsorbate/semiconductor bonding sites. However, without DFT computations it is challenging to make definitive bonding structure assignments for the adsorbate structures since STM does not provide elemental analysis on an atomic scale. DFT can be used to calculated enthalpies of adsorption of different bonding sites to determine the most stable bonding geometry. DFT can also be used to simulate STM images, thereby allowing confirmation of initial bonding geometry assignments. STM and DFT can also be used

to determine the electronic structure for semiconductors and/or adsorbate/semiconductor surfaces. The electronic structure of the adsorbate/semiconductor surface can be experimentally measured using scanning tunneling spectroscopy (STS). These spectra can then be compared to the computationally calculated density of states (DOS) to deduce correlations between the bonding sites of different adsorbates and the electronic structure of whole system.

To develop a molecular understanding of Fermi level pinning on GaAs(001)-$c(2\times8)/(2\times4)$, the bonding and electronic structures of four different adsorbates (O_2, In_2O, Ga_2O, and SiO) on GaAs(001)-$c(2\times8)/(2\times4)$ were studied. Previously performed STM studies by Kruse *et al.*,[9] Hale *et al.*,[10,11] and Winn *et al.*[12] detailed the bonding geometries of O_2, In_2O, Ga_2O, and SiO on the GaAs(001)-$c(2\times8)/(2\times4)$ surfaces. However, these studies were performed using a variety of theoretical techniques preventing careful comparison between the adsorbates. Section III A describes a new set of adsorbate/semiconductor DFT calculations using a consistent computational method for all four adsorbates, thereby enabling comparison to be made between the four different systems. Furthermore, several new bonding sites were modeled to ensure full comparison between all bonding geometries. Section III B presents STS data along with the DFT DOS calculations which elucidate the mechanisms, by which the four adsorbates perturb the electronic properties of GaAs(001)-$c(2\times8)/(2\times4)$. STS spectra show that the only adsorbate that leaves the Fermi level unpinned is Ga_2O. The DOS revealed that two distinct pinning mechanisms are present on GaAs(001)-$c(2\times8)/(2\times4)$, direct and/or indirect Femi level pinning.

[a)]Electronic mail: akummel@ucsd.edu

II. EXPERIMENTAL AND COMPUTATIONAL TECHNIQUES

The experiments were performed in an UHV chamber with a base pressure of 3×10^{-10} Torr. The chamber was equipped with low energy electron diffraction (LEED) and a Park Scientific VP STM with STS capabilities. As_2 capped *n*- and *p*-type GaAs wafers with Si and Be dopant concentrations of 2×10^{17} cm^{-3} were used for the Ga_2O and SiO experiments. For the O_2 and In_2O studies, wafers with dopant concentration of 2×10^{16} cm^{-3} were employed. The wafers were thermally decapped to the GaAs(001)-$c(2 \times 8)/(2 \times 4)$ reconstruction by performing annealing cycles to 420 °C. Cycles were continued until no pressure rise was observed during the ramp (typically 20 cycles). Details of the decapping procedure have been discussed elsewhere.[12] The surface periodicity was then verified by employing both LEED and STM. Variable tip-sample separation differential conductance (dI/dV) measurements were taken to confirm that the clean surface was unpinned. Subsequently O_2, In_2O, Ga_2O, or SiO was deposited onto the surface. An effusion cell was used to deposit the In_2O, Ga_2O, and SiO, while an UHV leak valve was employed for the O_2. Details of the deposition and dosing procedures are discussed elsewhere.[9–12] After deposition, the electronic properties of the system were evaluated using STS. STS measurements were taken by employing the variable tip-sample separation method developed by Feenstra and co-workers.[13–15]

DFT calculations were performed using the Vienna *ab initio* simulation package (VASP).[16–19] The adsorbate/surface systems were modeled using an eight layer GaAs(001) slab that was bottom terminated with H atoms having a $1.25e^-$ configuration. The bottom three layers of the slab along with the H atoms were frozen in bulk position to preserve the bulk properties of the system. These calculations were performed using the Perdew-Burke-Ernzerhof[20] (PBE) variation of the generalized gradient approximation. Atoms were modeled using projector augmented wave (PAW) potentials.[21,22] The plane wave cutoff energy was set to 400 eV and a $4 \times 4 \times 1$ Monkhorst-Pack[23] *k*-point sampling scheme was used, which resulted in the generation of four irreducible *k* points in the first Brillouin zone. The structures were considered fully relaxed when the interatomic forces were below 0.01 eV/Å. The calculations were assumed to be accurate within 0.10 eV; a more in-depth discussion on how the ±0.10 eV error value was reached is presented elsewhere.[12]

III. RESULTS AND DISCUSSION

A. Bonding sites and enthalpies of adsorption

All of the systems of interest have their bonding geometries well documented in literature.[9–12] Previous calculations performed on these systems could not be compared due to a lack of consistency in the computational methodologies. Figures 1–4 show top-down views of the previously determined experimentally observed sites for O_2, In_2O, Ga_2O, and SiO;[9–12] in addition, the consistently calculated enthalpies of adsorption per molecule are displayed. The structures that incorporate an undimerized As atom in them (O_2 single dimer displacements, SiO row compact double, SiO trough
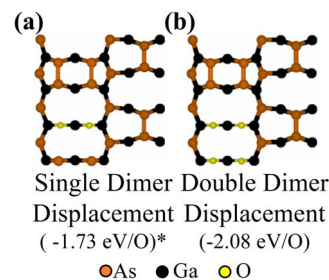

FIG. 1. (Color online) Top-down views of the lowest energy structures of O_2 bonded to the GaAs(001)-$c(2 \times 8)/(2 \times 4)$ surface: (a) single dimer displacement and (b) double dimer displacement. The adsorption energy per oxide molecule is displayed below each structure. The energy denoted with "*" has been corrected to include half the As dimerization energy for each undimerized As atom.

compact double, and SiO trough pyramid sites) have had their energies corrected by adding half the energy of an As dimer for every undimerized As atom in the calculation.

1. O_2 dissociative chemisorption

The DFT models of the two experimentally observed O sites are seen in Fig. 1. These sites include the single dimer displacement and the double dimer displacement sites. In these sites, either one or two O_2 molecules adsorb onto the
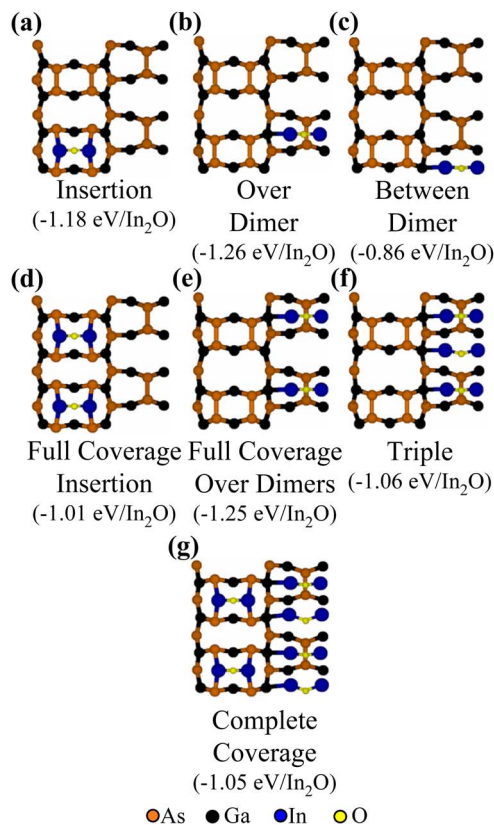

FIG. 2. (Color online) Top-down views of the lowest energy structures of In_2O bonded to the GaAs(001)-$c(2 \times 8)/(2 \times 4)$ surface: (a) row insertion, (b) trough over dimer, (c) trough between dimer, (d) row full coverage insertion, (e) trough full coverage over dimer, (f) trough triple, and (g) complete coverage. The adsorption energy per oxide molecule is displayed below each structure.
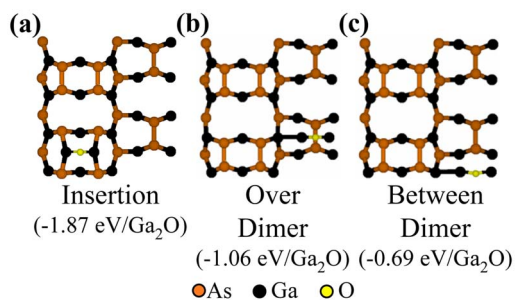
FIG. 3. (Color online) Top-down views of the lowest energy structures of Ga_2O bonded to the GaAs(001)-$c(2\times8)/(2\times4)$ surface: (a) row insertion, (b) trough over dimer, and (c) trough between dimer. The adsorption energy per oxide molecule is displayed below each structure.

surface and displace row As atoms that are adjacent to each other. This process generates excess As atoms on the surface. From the enthalpies of adsorption, it can be seen that the double dimer displacement [Fig. 1(b)] is only slightly more favorable (by 0.35 eV/O) than the single dimer displacement [Fig. 1(a)]. Kruse et al.[9] experimentally showed that when GaAs(001)-$c(2\times8)/(2\times4)$ is exposed to O_2, the surface contains a mixture of the two sites. One critical difference exists between the two sites; the single dimer displacement causes the formation of two undimerized As atoms, while the double dimer displacement site does not.

2. In_2O *chemisorption on rows and troughs*

Hale et al.[10] showed that when In_2O was deposited onto GaAs(001)-$c(2\times8)/(2\times4)$ at 400 °C, even at low coverage, bonding sites formed in both the row and trough regions. At ~1 ML In_2O coverage, the average spacing be-
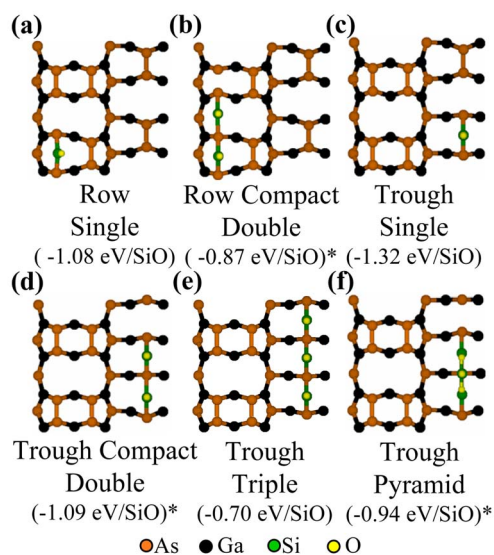

FIG. 4. (Color online) Top-down views of the lowest energy structures of SiO bonded to the GaAs(001)-$c(2\times8)/(2\times4)$ surface: (a) row single, (b) row compact double, (c) trough single, (d) trough compact double, (e) trough triple, and (f) trough pyramid. The adsorption energy per oxide molecule is displayed below each structure. The energies denoted with " *" have been corrected to include half the As dimerization energy for each undimerized As atom.

tween In_2O molecules was greater than 24 Å, revealing that the In_2O molecules had no affinity for clustering.

The enthalpies of adsorption of the seven In_2O bonding sites considered in this study are given in Fig. 2. Three of the sites are considered single sites because they only contain one In_2O molecule: row insertion [Fig. 2(a)], trough over dimer [Fig. 2(b)], and trough between dimer [Fig. 2(c)] sites. The insertion site occurs when an In_2O molecule inserts into a row As dimer. The trough sites occur when an In_2O molecule forms a bridge bond across the trough; the In_2O molecules can be positioned over the trough As dimers [trough over dimer site, Fig. 2(b)] or it can be positioned between two trough As dimers [trough between dimer site, Fig. 2(c)].

The sites remaining are combination sites and are formed by combining multiple single sites: row full coverage insertion [Fig. 2(d)], trough full coverage over dimers [Fig. 2(e)], trough triple [Fig. 2(f)], and complete coverage [Fig. 2(g)] sites. The adsorption energies of the combination sites show that clustering of In_2O molecules has no effect on the adsorption energy. Therefore, only three sites need to be considered when discussing adsorption energies: row insertion, trough over dimer, and trough between dimer sites.

The adsorption energies of the three single sites show that the row insertion and trough over dimer sites are energetically degenerate within the error range of these calculations. These results are consistent with experimental findings that both row and trough sites form even at low coverage. The trough between dimer site is ~0.29 eV less stable than the row insertion and trough over dimer sites. Therefore, it is expected that the row insertion and trough over dimer sites will fill in before the trough between dimer sites starts forming.

Hale et al. suggested that the In_2O molecules might be able to bond both O end up and down in the trough region.[10] Multiple attempts were made to find stable structures for the trough over dimer and trough between dimer sites that had O atoms bonded downward into the trough. While no truly stable bonding geometries were found for these configurations, a weak metastable structure was found for the O down trough between dimer site. In order for the In_2O molecule to bond O down between trough dimers, it was necessary to have two other In_2O molecules bonded O end up over adjacent trough dimers, to prevent the In_2O molecule from flipping over in order to orient the O upwards. The adsorption energy for solely the "trapped" O down trough between dimer site was found to be only −0.57 eV. Therefore, it is not clear what role, if any, this site plays in the final bonding geometry picture.

The In_2O adsorption energies show that it is always energetically preferable to have an In_2O molecule bonded over a trough dimer than between trough dimers. This difference in energy is most likely a result from interactions between the filled dangling bonds on the As trough dimers and the oxide molecule. The interaction is more severe in the between dimer site since the majority of the electron density in the filled dangling bonds is located in this position.
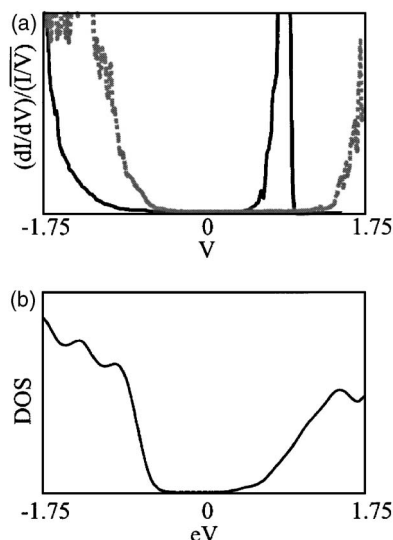
FIG. 5. (a) STS measurements of the clean *n*-type (black solid line) and *p*-type (gray dashed line) GaAs(001)-$c(2\times8)/(2\times4)$ surfaces. (b) Calculated DOS for the clean surface.

3. Ga$_2$O *chemisorption on rows and troughs*

Although one might predict that Ga$_2$O bonding on GaAs(001)-$c(2\times8)/(2\times4)$ would be similar to In$_2$O bonding to GaAs(001)-$c(2\times8)/(2\times4)$, there are actually major differences between these two isoelectronic systems. The STM images taken by Hale *et al.*[11] of Ga$_2$O deposited onto GaAs(001)-$c(2\times8)/(2\times4)$ showed that the initial bonding site for the Ga$_2$O molecules was to insert into the row As dimers. Unlike In$_2$O, no low coverage trough sites were ever experimentally observed.

The high coverage results for Ga$_2$O were also distinctly different than those for In$_2$O. At high coverage (~1 ML), the Ga$_2$O molecules were found to form parallel rows on the surface with the most common row spacing being ~8 Å. This result suggests that unlike In$_2$O, Ga$_2$O has an affinity for clustering. The ~8 Å, Ga$_2$O row spacing yielded a (2×2) surface periodicity. The typical separation between the As dimer rows on the GaAs(001)-$c(2\times8)/(2\times4)$ surface is ~16 Å. Therefore, in order to form an ~8 Å row spacing, the surface would need to undergo a surface reconstruction. Experimentally, it was observed that as the concentration of Ga$_2$O on the surface increased, the number of steps also increased. It was assumed that this step formation generated the needed As atoms to allow for the (2×2) reconstruction to form. Even though the majority of the In$_2$O molecules were found to have a row spacing of greater than 24 Å, a small number of In$_2$O molecules were found with a row spacing of ~8 Å. This suggest that small areas of the In$_2$O surface also might have undergone some rearrangement.[10]

Calculations reveal that the row insertion site [Fig. 3(a)] is -1.87 eV exothermic, consistent with the low coverage experimental results. In addition, the adsorption energies of two trough sites were calculated for comparison with In$_2$O bonding sites. Although the trough sites were not observed with STM, the stability of the trough over dimer and trough between dimer sites (-1.06 and -0.69 eV, respectively) indicates that the trough filling mechanism is probably more complex than a simple As rearrangement.
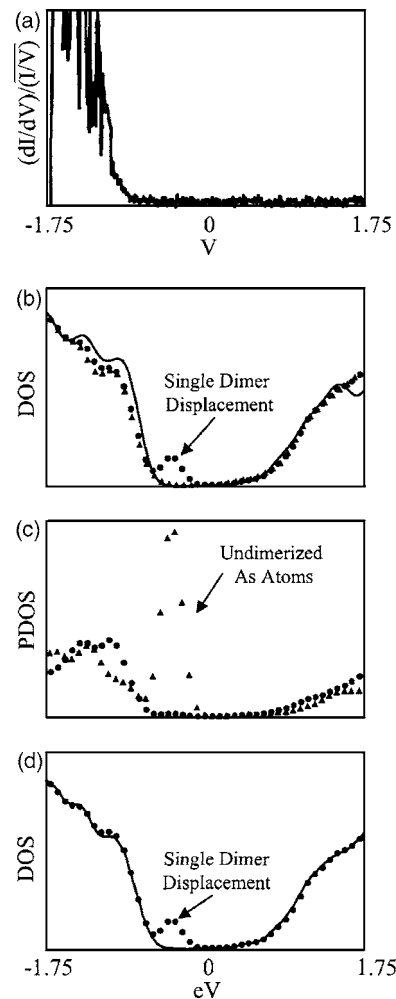

FIG. 6. (a) STS measurement of O$_2$ adsorbed onto *n*-type GaAs(001)-$c(2\times8)/(2\times4)$. (b) DOS calculations of O$_2$ sites: clean surface (thick bold line), single dimer displacement (●), and double dimer displacement (▲). (c) PDOS calculations showing the average of the surface As atoms that are dimerized (●) vs the average of the surface As atoms that are not dimerized (▲). (d) DOS calculations of the unpassivated single dimer displacement (●) and the single dimer displacement with the undimerized As atoms passivated with H atoms (thick bold line).

Calculations were also attempted on a Ga$_2$O down trough sites but no stable/metastable sites were found. This was attributed to the fact that the Ga$_2$O molecules are slightly smaller than the In$_2$O molecules, which enables them to rotate into the energetically preferred position of O up, regardless of the surrounding environment.

In an effort to understand the energy discrepancy between the trough and row sites, an in-depth look must be taken at the fundamental bonding properties of the systems. On GaAs(001)-(2×4), when the Ga$_2$O inserts into the row, Ga–As bonds are created; conversely when Ga$_2$O bonds in the trough, Ga–Ga bonds are created. In covalent compounds, Ga–Ga bonds are $\sim1/2$ as stable as Ga–As bonds.[24] The other major difference between the row and trough sites is that four bonds are created when each row insertion site is formed and only two bonds are created when either of the two trough sites is formed.

Not only is it important to understand what bonding sites will be occupied but it is also equally important to under-
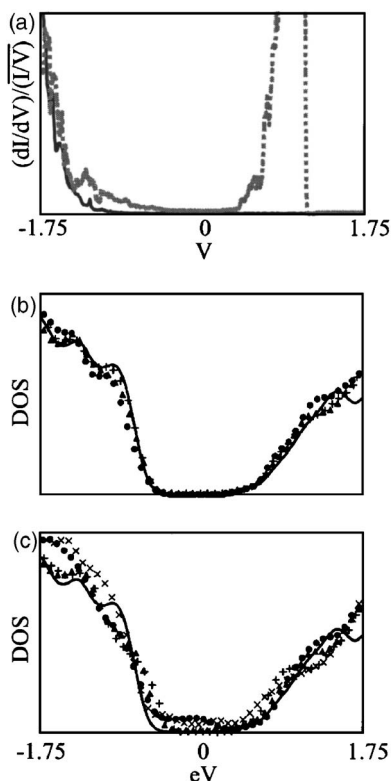
FIG. 7. (a) STS measurements of In$_2$O adsorbed onto n-type (black line) and p-type (gray dashed line) GaAs(001)-$c(2\times8)/(2\times4)$. (b) DOS calculations of In$_2$O sites: clean surface (black line), insertion (●), over dimer (▲), and between dimer (+). (c) DOS calculations of combination sites: row full coverage insertion (●), trough full coverage over dimers (▲), trough triple (+), and complete coverage (×).

FIG. 8. (a) STS measurements of Ga$_2$O adsorbed onto n-type (black line) and p-type (gray dashed line) GaAs(001)-$c(2\times8)/(2\times4)$. (b) DOS calculations of Ga$_2$O sites: clean surface (thick bold line), row insertion (●), trough over dimer (▲), and trough between dimer (+) sites.

stand energetic differences between the In$_2$O and Ga$_2$O bonding sites on the GaAs(001)-$c(2\times8)/(2\times4)$ surface. The Ga$_2$O trough site energies are comparable to the In$_2$O trough sites energies. However, the Ga$_2$O row insertion site is significantly more stable than the In$_2$O row insertion site (-1.87 vs -1.18 eV, respectively). The difference in stability between the row insertion sites results from Ga–As and In–As bond strength differences. In order to estimate the approximate bond strength difference of Ga–As and In–As bonds, plane wave calculations were performed to get the enthalpies of reaction for the following two reactions using VASP:

$$Ga_2OAs_4H_8 + 2H_2 \rightarrow Ga_2O + 4AsH_3, \tag{1}$$

$$In_2OAs_4H_8 + 2H_2 \rightarrow In_2O + 4AsH_3. \tag{2}$$
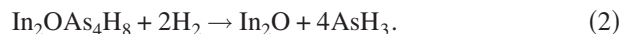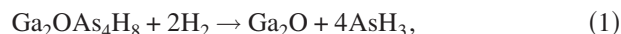
The difference in enthalpies of reaction is equal to four times the difference in bond energies between Ga–As and In–As bonds; this was calculated to be 0.57 eV. This value is comparable to the Ga$_2$O and In$_2$O insertion site energy differences (0.69 eV). Therefore, it can be concluded that the main difference between these two systems arises from the bond strengths.

4. SiO chemisoption on rows and troughs

Six bonding sites are experimentally observed at low coverage for SiO deposited on GaAs(001)-$c(2\times8)/(2\times4)$
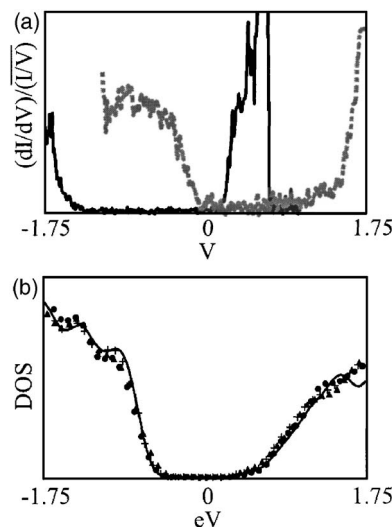
(Fig. 4). These sites include row and trough single [Figs. 4(a) and 4(c), respectively], row and trough compact double [Figs. 4(b) and 4(d), respectively], trough triple [Fig. 4(e)], and trough pyramid [Fig. 4(f)] sites. The row and trough single sites form when a SiO molecule inserts into an As–As dimer bond in either the row or trough. If an additional SiO molecule inserts between a single site and an adjacent dimer, then the site is referred to as a row or trough compact double site. There are two more complex bonding geometries that are only found in the trough region: trough triple and trough pyramid sites. The trough triple site forms when two trough single sites bond in adjacent dimers and an additional SiO molecule bonds between the two occupied dimers. In order for a trough pyramid site to form, a trough compact double site forms, and subsequently, an additional SiO molecule bonds on top, forming a pyramid. A detailed investigation of these bonding sites along with a chemical potential plot showing that all of these geometries are viable bonding sites, depending on the SiO coverage, is presented elsewhere.[12] The trough sites were found to be slightly more favorable than their row counterparts. This was attributed to stabilization received from the dangling bonds of the Ga atoms that protrude into the trough. In addition, the stabilization received from the dangling bonds of the Ga atoms allows the more complex sites (trough triple and trough pyramid sites) to form in the trough region.

B. Scanning tunneling spectroscopy and density of states measurements

Surface electronic measurements were taken of the different systems using STS. For all STS measurements, the Fermi level resides at 0 V. Figure 5(a) shows $(dI/dV)/(\overline{I/V})$ vs V measurements, which are proportional to the surface DOS of the clean n- and p-type surfaces.[25] The Fermi level resides near the conduction band for the clean, oxide-free
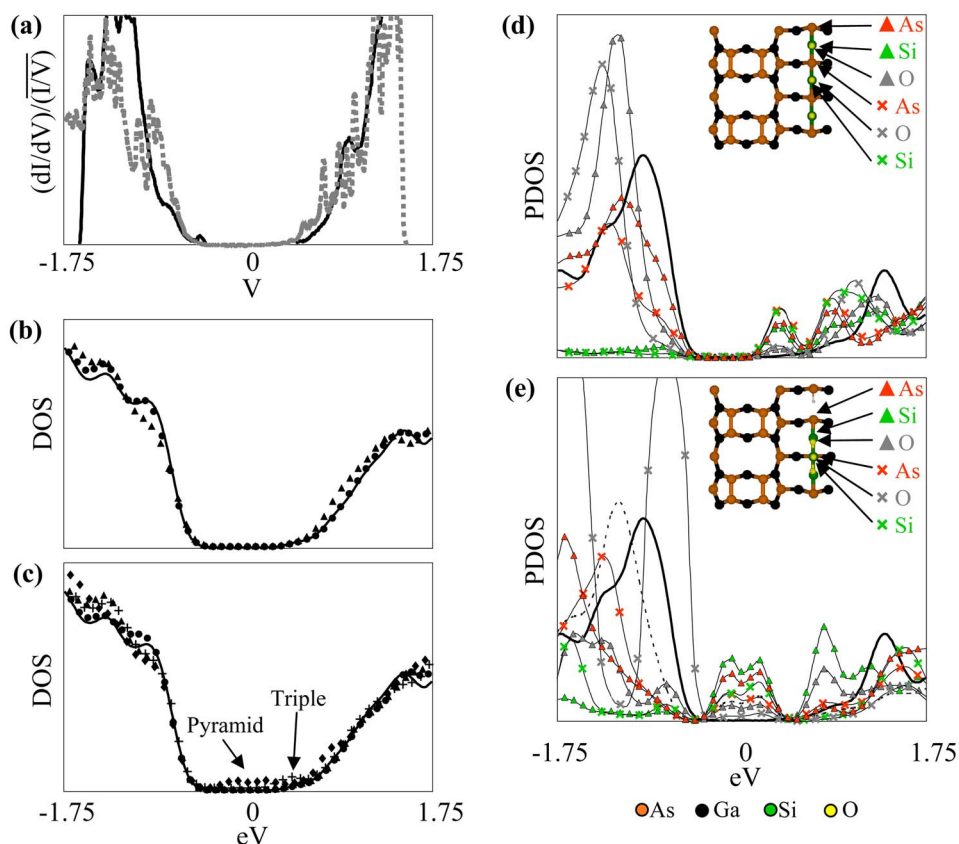
FIG. 9. (a) (Color online) STS measurements of SiO adsorbed onto *n*-type (black bold line) and *p*-type (gray dashed line) GaAs(001)-$c(2\times8)/(2\times4)$. (b) DOS calculations of the row SiO sites: clean surface (thick bold line), row single (●), and row compact double (▲). (c) DOS of the trough SiO sites: clean surface (thick bold line), trough single (●), trough compact double (▲), trough triple (+), and trough pyramid (♦). (d) PDOS calculations for the trough triple sites; atoms which PDOS have been plotted for are labeled in the ball-and-stick diagram in the upper right hand corner of the plot; the thick black line is a PDOS of a trough As dimer on the clean surface for comparison. (e) PDOS calculations for the trough pyramid sites; atoms which PDOS have been plotted for are labeled in the ball-and-stick diagram in the upper right hand corner of the plot; the thick black line is a PDOS of a trough As dimer on the clean surface and the dashed line is the As atom with the H bonded to it.

n-type surface and resides near the valence band for the clean oxide-free *p*-type surface, typical of an unpinned surface.

DOS calculations were also performed on the clean surface [Fig. 5(b)] as well as the oxide covered surfaces. These calculations differ from STS measurements in two major ways. First, the computational slabs are not large enough to be doped; therefore, the computational slabs are intrinsic. Second, the position of the Fermi level within the band gap is somewhat arbitrary in DFT; therefore, in all the DFT calculations the DOSs have been aligned using the deep level states. Regardless of these differences, if the calculated DOS shows adsorbate induced states within the band gap region, it can be reasonably concluded that the adsorbate would cause the experimental surface to be pinned.

1. O₂ *chemisorbate electronic structure*

Figure 6(a) shows a STS measurement of *n*-type sample after ~900 L exposure to O_2. The conduction band is not observed for this *n*-type sample due to the low dopant concentration of the wafer, which prohibits complete inversion from being obtained during the STS measurement.[26] The STS measurement reveals that the bands have bent causing

the Fermi level to be located midgap (~0.7 V from the valence band edge); this is typical of a pinned sample. Although no *p*-type STS spectra are presented in this paper, other groups have verified that exposing O_2 to GaAs pins the Fermi level.[27,28]

To deduce the cause of the Fermi level pinning seen experimentally, DOS and projected density of states (PDOS) calculations were performed. Figure 6(b) presents the calculated DOS for a surface containing two O atoms that have replaced two As atoms, and a surface containing four O atoms that have replaced four As atoms. The DOS of the clean surface is also displayed for comparison. The plots reveal that states are only generated in the band gap region when two O atoms replace two As atoms. To further investigate which atoms contribute to the states in the DOS, PDOS calculations were performed. PDOS calculations for the surface As atoms are seen in Fig. 6(c). The PDOS reveals that the major contributors to the midgap states are the undimerized As atoms. This also rationalizes why no states are observed in the band gap region when four O atoms replace four As atoms because no undimerized As atoms are generated. This suggests that the properties of the O atoms do not directly cause Fermi level pinning on the GaAs(001)-$c(2\times8)/(2\times4)$ surface; instead, the pinning is most likely due to the

TABLE I. Summary of the different adsorbate bonding sites along with adsorbate induced changes in the surface electronic structure: unpinned, directly pinned, or indirectly pinned.

	Unpinned or cause of pinning
O_2	
Single dimer displacement	Indirect
Double dimer displacement	Unpinned
In_2O	
Insertion	Unpinned
Over dimer	Unpinned
Between dimer	Unpinned
Full coverage insertion	Direct
Full coverage over dimers	Direct
Triple	Direct
Complete coverage	Direct
Ga_2O	
Insertion	Unpinned
Over dimer	Unpinned
Between dimer	Unpinned
SiO	
Row single	Unpinned
Row compact double	Indirect
Trough single	Unpinned
Trough compact double	Indirect
Trough triple	Direct
Trough pyramid	Direct

generation of undimerized As atoms. Therefore, the pinning mechanism is considered to be indirect. Previous reports incorrectly attributed the pinning to a direct mechanism, but this was due to inferior or incorrect computational methods.[29]

On real (experimental) surfaces, the undimerized As atoms may be able to redimerize, thereby eliminating the midgap As states, if two criteria are met. First, the activation barrier must be low enough to allow for the reconstruction of the row, in order to facilitate the redimerization of the As atoms. Second, there must be another undimerized As atom in the same row to terminate the process with a complete dimer. Although it might be possible to meet both of these constraints, the second criteria become harder to fulfill on smaller terraces. If these criteria cannot be met, and undimerized As atoms remain on the surface, the Fermi level is expected to be pinned.

H atoms can be used to (computationally) passivate these undimerized As atoms in order to verify that they are the only cause of O induced states. Figure 6(d) displays the DOS for a surface containing two O atoms and two undimerized As atoms and a surface containing two O atoms with the undimerized As atoms passivated with H atoms. The plot clearly shows that the H passivation suppresses the states in the band gap region, yielding a DOS that is similar to the clean unpinned surface. This result indicates that it is the resultant dangling bonds on the undimerized As atoms that cause the observed Fermi level pinning. This result also indicates that H passivation can be used for any system that

has undimerized As atoms; once the H atoms have been used to passivate the undimerized As atoms, any states left in the band gap region are a direct result of the adsorbate bonding with the surface.

2. In_2O *chemisobate electronic structure*

STS results of In_2O on GaAs(001)-$c(2 \times 8)/(2 \times 4)$ are presented in Fig. 7(a). Although the n-type sample has the same STS spectra as the unpinned surface, the p-type sample clearly shows that the In_2O deposited on GaAs(001)-$c(2 \times 8)/(2 \times 4)$ causes the Fermi level to be pinned near the conduction band edge.

The DOS of the In_2O single sites (row insertion, trough over dimer, and trough between dimer) in Fig. 7(b) shows that none of these sites induce states in the band gap region. Although the single sites do not cause state formation in the band gap, all of the combination sites (row full coverage insertion, trough full coverage over dimers, trough triple, and complete coverage) induce states into the band gap region, as shown in Fig. 7(c). As the coverage on the row increases from the row insertion site to the full coverage insertion site, state formation is seen in the band gap region. Similarly, as the trough coverage increases form the single trough sites to the trough full coverage over dimer site, and finally to the trough triple site, the state density in the band gap region also increases. These results suggest that the higher the In_2O coverage, the greater the state formation in the band gap. This was further substantiated by the DOS for the experimentally observed high coverage site (complete coverage in which every available site is filled), which has the highest state formation in the band gap region of all the sites. A PDOS analysis revealed that the pinning states were delocalized and existed throughout the top four layers of the slab.

Hale *et al.* reported that room temperature deposition resulted in In_2O molecules inserting into missing As row dimers (defect sites).[10] Calculations were performed on this geometry and the site was shown to only be marginally stable (−0.33 eV). The DOS revealed that these empty dimer sites generated states in the band gap. However, it is not believed that this site plays a major role in the Fermi level pinning since the concentration of these sites is very low.

In_2O pinning is distinct from pinning by the other oxides (O_2 and SiO) on GaAs(001)-$c(2 \times 8)/(2 \times 4)$ because In_2O experimentally pins the Fermi level near the conduction band edge, while the other oxides experimentally pin the Fermi level midgap. Although states generated in the band gap region are distinctly different depending on whether multiple row or multiple trough sites caused the formation, both types of states can be evaluated to understand why In_2O pins the Fermi level near the conduction band. Multiple row insertion sites induce states that start at the valence band edge and extend toward the conduction band, residing in over half of the band gap region. Analysis of the Kohn-Sham orbital occupancies indicates that these are filled states. These results imply that the Fermi level should indeed be pinned near the conduction band edged inside the reduced band gap. The states that are generated when the coverage increases and multiple trough sites are forced to form in close proximity to each other are located at both the valence and conduction

TABLE II. Table showing the new data and calculations presented in this paper and comparisons to other published data discussed in the paper.

	O_2	In_2O	Ga_2O	SiO
Adsorption sites	Identical to Ref. 11.	Similar to Ref. 10. Additional computations were performed to identify coverage effects.	Similar to Ref. 11 Additional computations were performed to identify coverage effects and examine trough sites.	Identical to Ref. 12.
Level of theory	Old=LDA Ultrasoft pseudopotentials New=PBE PAW potentials Higher accuracy	Old=LDA Ultrasoft pseudopotentials New=PBE PAW potentials Higher accuracy	Old=LDA Ultrasoft pseudopotentials New=PBE PAW potentials Higher accuracy	Identical to Ref. 12.
STS	Different spectra but identical interpretation to Ref. 11.	New	Different spectra but identical interpretation to Ref. 11	Identical to Ref. 12.
DOS	New[a]	New	New[a]	Identical to Ref. 12.
Interpretation	New[a]	New	Identical to Ref. 11.	Identical to Ref. 12.

[a]For these calculations, discrepancies between the current manuscript and Ref. 11 come from computational errors that were outlined in a published erratum (Ref. 29).

band edges. Although it is clear that these states play a role in the Fermi level pinning, it is difficult to conclude exactly where the Fermi level should reside as a result.

3. Ga_2O chemisorbate electronic structure

Experimental and calculated electronic structures of Ga_2O on GaAs(001)-$c(2\times8)/(2\times4)$ are displayed in Fig. 8. STS measurements [Fig. 8(a)] show that the Fermi level resides close to the conduction band for n-type samples and close to the valence band for p-type samples, revealing that Ga_2O leaves the GaAs(001)-$c(2\times8)/(2\times4)$ surface unpinned. These findings were further substantiated by the fact that the calculated DOS [Fig. 8(b)] for the insertion site had no states in the band gap region. The DOSs for the trough over dimer and trough between dimer sites are also displayed in Fig. 8(b), for comparison with the In_2O system. Although these sites are not explicitly seen experimentally, the DOS reveals that both the Ga_2O troughs between dimer and trough over dimer sites also have no states in the band gap region.

The Ga_2O insertion site leaves the Fermi level unpinned because the insertion site does not trigger any chemical event which causes Fermi level pinning. In contrast to O_2 chemisorption on the GaAs(001)-$c(2\times8)/(2\times4)$ surface, the Ga_2O insertion site does not cause the generation of undimerized As atoms nor does it cause the generation of excess As atoms. In addition, when a Ga_2O molecule bonds on the row, the filled dangling bonds on the row As atoms are preserved, and no extra dangling bonds are introduced.

The electronic effects of increased coverage were also computationally explored for Ga_2O on GaAs(001)-$c(2\times4)$. Similar to In_2O, all of the higher coverage Ga_2O sites pinned the Fermi level. However, the simulated high coverage sites for Ga_2O do not represent the experimental surface since they do not result in a (2×2) surface reconstruction. Therefore, these results are not relevant to the examination of the electronic properties of Ga_2O on GaAs(001)-$c(2\times8)/(2\times4)$.

Calculations were also performed for a Ga_2O molecule inserting into a missing As row dimer. Similar to the In_2O case, this site was also found to induce states into the band gap region. In addition, the bonding geometry was found to be significantly more stable for Ga_2O than for In_2O (-0.42 eV more stable). Therefore, since Ga_2O was experimentally shown to leave the Fermi level unpinned, the number of defect sites must be small enough to not play a major role in the electronic properties of the system.

4. SiO chemisorbate electronic structure

STS of SiO on GaAs(001)-$c(2\times8)/(2\times4)$ is presented in Fig. 9(a). The STS results reveal that SiO deposition on GaAs experimentally pins the Fermi level at midgap. The calculated DOSs for the row and trough adsorption sites are seen in Figs. 9(b) and 9(c), respectively. The DOSs have H atoms passivating any undimerized As atoms that were generated by the bonding sites, leaving only the states directly induced by the SiO molecules. These DOSs show that only two of the six geometries (trough triple and pyramid sites)

directly induce states in the band gap region. These results are consistent with the experimental findings. In addition, the compact double sites and the pyramid site generate undimerized As atoms, which most likely play an indirect role in the Fermi level pinning.

PDOS analysis was performed on the trough triple [Fig. 9(d)] and trough pyramid [Fig. 9(e)] sites to deduce the causes of state formation in the band gap region for SiO bonded to the GaAs(001)-$c(2 \times 8)/(2 \times 4)$ surface. The PDOS from the trough triple site [Fig. 9(d)] shows that the states observed near the conduction band edge in the DOS reside on the surface As, Si, and O atoms. A Bader style atomic charge analysis[30] revealed that the likely cause of the band gap states in the trough triple site was from a local buildup of charge on multiple adjacent As atoms. Similar to the PDOS of the trough triple site, the trough pyramid site PDOS [Fig. 9(e)] reveals that the band gap states also reside on the surface As, Si, and O atoms. The band gap states were attributed to the generation of partially filled dangling bonds on the bottom Si atoms of the trough pyramid site. A more in-depth study of the SiO/GaAs(001)-$c(2 \times 8)/(2 \times 4)$ surface is presented elsewhere.[12]

The study of the four adsorbates showed that on GaAs(001)-$c(2 \times 8)/(2 \times 4)$ there are two distinct mechanisms of Fermi level pinning (direct and/or indirect). Table I shows a list of all of the bonding sites that were calculated along with their perturbation of the electronic structure: Fermi level unpinned, Fermi level pinned directly, or Fermi level pinned indirectly. In addition since this paper drew heavily from previous publications, Table II outlines the experimental data that were taken from other papers along with how the DFT calculations published in this paper differ from the DFT calculations published in previous publications.

IV. CONCLUSION

Experimental results revealed that out of the four adsorbates studied (O_2, In_2O, Ga_2O, and SiO) only one, Ga_2O, left the Fermi level unpinned when it bonded to GaAs(001)-$c(2 \times 8)/(2 \times 4)$. DFT simulations were used to explain the different pinning mechanisms for other adsorbates. The mechanisms can be broken down into two general categories: direct and indirect. Direct Fermi level pinning results when the bonding between the adsorbate and the surface directly induces states into the band gap region. In comparison, indirect Fermi level pinning occurs when states are induced in the band gap region because of secondary effects, such as the generation of undimerized As atoms. Since indirect pinning is not caused by the properties of the adsorbates themselves, it may be possible to create unpinned surfaces using H passivation or even a multilayer of oxide. Adsorbates that cause Fermi level pinning on GaAs(001)-$c(2 \times 8)/(2 \times 4)$ can either exhibit one of the pinning mecha-

nisms [O (indirect) and In_2O (direct)] or they can exhibit both of the mechanisms (SiO). In addition, the close correlation between experiment and theory in this study suggests that DFT can be used on other III-V semiconductor systems to predict oxide pinning and unpinning.

[1] N. Yokoyama, T. Mimura, and M. Fukuta, IEEE Trans. Electron Devices **27**, 1124 (1980).
[2] J. Y. Wu, H. H. Wang, Y. H. Wang, and M. P. Houng, IEEE Trans. Electron Devices **48**, 634 (2001).
[3] Y. C. Wang, M. Hong, J. M. Kuo, J. P. Mannaerts, J. Kwo, H. S. Tsai, J. J. Krajewski, Y. K. Chen, and A. Y. Cho, IEEE Electron Device Lett. **20**, 457 (1999).
[4] H. Takagi, G. Kano, and I. Teramoto, IEEE Trans. Electron Devices **25**, 551 (1978).
[5] C. J. Huang, Z. S. Ya, J. H. Horng, M. P. Houng, and Y. H. Wang, Jpn. J. Appl. Phys., Part 1 **41**, 5561 (2002).
[6] A. Colquhoun, E. Kohn, and H. L. Hartnagel, IEEE Trans. Electron Devices **25**, 375 (1978).
[7] K. Rajagopalan, J. Abrokwah, R. Droopad, and M. Passlack, IEEE Electron Device Lett. **27**, 959 (2006).
[8] K. Rajagopalan, R. Droopad, J. Abrokwah, P. Zurcher, P. Fejes, and M. Passlack, IEEE Electron Device Lett. **28**, 100 (2007).
[9] P. Kruse, J. G. McLean, and A. C. Kummel, J. Chem. Phys. **113**, 9224 (2000).
[10] M. J. Hale, J. Z. Sexton, D. L. Winn, A. C. Kummel, M. Erbudak, and M. Passlack, J. Chem. Phys. **120**, 5745 (2004).
[11] M. J. Hale, S. I. Yi, J. Z. Sexton, A. C. Kummel, and M. Passlack, J. Chem. Phys. **119**, 6719 (2003).
[12] D. L. Winn, M. J. Hale, T. J. Grassman, A. C. Kummel, R. Droopad, and M. Passlack, J. Chem. Phys. **126**, 084703 (2007).
[13] P. Martensson and R. M. Feenstra, Phys. Rev. B **39**, 7744 (1989).
[14] R. M. Feenstra and J. A. Stroscio, J. Vac. Sci. Technol. B **5**, 923 (1987).
[15] R. M. Feenstra, Phys. Rev. B **50**, 4561 (1994).
[16] G. Kresse and J. Hafner, Phys. Rev. B **47**, 558 (1993).
[17] G. Kresse, thesis Technische University at Wien, 1993.
[18] G. Kresse and J. Furthmüller, Comput. Mater. Sci. **6**, 15 (1996).
[19] G. Kresse and J. Furthmüller, Phys. Rev. B **54**, 11169 (1996).
[20] J. P. Perdew, K. Burke, and M. Ernzerhof, Phys. Rev. Lett. **77**, 3865 (1996).
[21] P. E. Blochl, Phys. Rev. B **50**, 17953 (1994).
[22] G. Kresse and J. Hafner, J. Phys.: Condens. Matter **6**, 8245 (1994).
[23] H. J. Monkhorst and J. D. Pack, Phys. Rev. B **13**, 5188 (1976).
[24] *Handbook of Chemistry and Physics*, 87th ed. (CRC, Boca Raton, FL, 2006).
[25] R. M. Feenstra, J. A. Stroscio, and A. P. Fein, Surf. Sci. **181**, 295 (1987).
[26] R. Maboudian, K. Pond, V. Bresslerhill, M. Wassermeier, P. M. Petroff, G. A. D. Briggs, and W. H. Weinberg, Surf. Sci. **275**, L662 (1992).
[27] J. A. Stroscio, R. M. Feenstra, and A. P. Fein, Phys. Rev. Lett. **58**, 1668 (1987).
[28] J. A. Stroscio, R. M. Feenstra, and A. P. Fein, Phys. Rev. B **36**, 7718 (1987).
[29] M. J. Hale, S. I. Yi, J. Z. Sexton, A. C. Kummel, and M. Passlack, J. Chem. Phys. **127**, 049902 (2007).
[30] G. Henkelman, A. Arnaldsson, and H. Jonsson, Comput. Mater. Sci. **36**, 354 (2006).